JOURNAL OF MATERIALS SCIENCE 28 (1993) 3816–3822

Electrical transport in light rare-earth molybdates

KANCHAN GAUR, MADHURI SINGH, H. B. LAL
Department of Physics, University of Gorakhpur, Gorakhpur-273009, India

Rare-earth molybdates of the type $R_2(MoO_4)_3$ with R = La, Ce, Pr, Nd, Sm and Eu were prepared and characterized, and the electrical conductivity, σ and Seebeck coefficient, S in the temperature range 450–1200 K were measured. These molybdates are concluded to be insulating solids with a band gap which increases slowly going down the series from 2.30 eV for La molybdate to 3.20 eV for Eu molybdate. The plots of $\log \sigma$ and S versus T^{-1} show, in general, three linear regions with two break temperatures T_1 and T_2 occurring due to a change in the conduction mechanism. At higher temperatures the intrinsic conduction in these solids occurs via a band mechanism. The O^{2-}:2p and Mo^{6+}:4d orbitals form the valence and conduction bands, respectively. These bands are the main support of conduction in La, Sm and Eu molybdates; however, for Ce, Pr and Nd molybdates $4f^n$ levels fall within the band gap and become very effective in electrical conduction. The main charge-carrying entities seem to be electrons in Ce, Pr and Nd molybdates and holes in La, Sm and Eu molybdates. On the basis of mobility calculations of charge carriers it is concluded that the charge carriers in these bands become polarons which are, in fact, the charge carrying entities. At lower temperatures electrical conduction is mainly extrinsic. Cerium molybdate shows a semiconductor–semimetal transition around 940 K.

1. Introduction

Molybdates of the type $R_2(MoO_4)_3$ (where R = Sc, Y and La to Lu) are one of the important compounds of rare-earth elements. Some of these compounds show interesting piezoelectric, ferroelectric, ferroelastic, fluorescent and non-linear optical properties [1–10]. The interest in these compounds is recent; it is only in the last two decades that reasonably pure rare-earth molybdates have been prepared, identified and studied. Some of the authors and their coworkers have undertaken a study into the magnetic, dielectric and electrical transport properties of rare-earth compounds such as sesquioxides [11–13], tungstates [14–19], garnets [20, 21], alloys [22, 23], orthochromites [24, 25], vanadates [26, 29] and molybdates [30–35]. The present work reports electrical transport studies on polycrystalline La–Eu molybdates in the temperature interval 450–1200 K.

$R_2(MoO_4)_3$ compounds crystallize in a variety of structures depending upon the method of their preparation, the annealing temperature used and the rare-earth ionic radius. The details are given elsewhere [10]. Light rare-earth molybdates (La–Eu) occur in the α-form, which is of monoclinic [α-$Eu_2(WO_4)_3$] type, with a space group, C_2/c, with four molecules per unit cell [6, 10]. A rare-earth ion in such an arrangement is surrounded by twelve oxygen ions at the corners of a slightly distorted cubic cell.

2. Preparation and characterization of materials and experimental techniques

The materials were prepared as described in earlier publications [28, 32]. They were characterized by taking X-ray diffraction (XRD) patterns using CuK_α radiation. All the peaks are assigned definite *hkl* values on the basis of reported unit-cell parameters, which indicate that preparation of these materials from their respective sesquioxides and MoO_3 is complete. The measurements of electrical conductivity and the Seebeck coefficient were made on pressed pellets sintered for 40 h at around 1000 K. A two-electrode method was employed. Silver foils were used as the electrode material. The measurement details are described elsewhere [19, 29, 36, 37].

3. Results and discussion

Measurements of σ and S were performed on pressed pellets because it is extremely difficult to grow a large, purely α-phase, single crystal of these compounds; the hygroscopic character of these compounds makes it still more difficult. In polycrystalline pellets, grain boundaries and air pores considerably reduce the electrical conductivity, and conductivity measurements on them generally do not reflect the bulk value for the material. It is not possible to eliminate the grain boundaries and included pores completely; however, the pellets can be prepared in such a way that their influence is considerably reduced. With clean grain boundaries, the bulk value for the material can be obtained by suitable corrections for the porosity. The first requirement in this direction is to make pellets of uniform density. This was achieved by using a proper steel die and keeping the ratio of the square of the

0022–2461

thickness, t^2 to the face area, A, less than 4 as prescribed by other workers [36, 38]. Air pores are considerably reduced by making use of fine-grain powders and higher pelletizing pressure, P, and sintering the pellets around 700 K for 40–50 h. Pellets made at $P > 8 \times 10^8$ N-m^{-2} have a density, d_p, equal to 80–83% of the density, d_0, calculated from X-ray data. From the density data the single-crystal value of electrical conductivity, σ was obtained from the measured value σ_p using a relation described in [19]. The grain-boundary effect in pellets made at such high pressure is also considerably reduced. This is evident from the independence of σ (alternating current) on signal frequency $f = 50$–10^4 Hz. The electrodes on the pellet faces also play a significant role in the σ and S measurements. Ohmic contact between the pellet and electrode interface is a stringent criterion [38]. It was checked that platinum-foil electrodes form ohmic contact with the pellets of all molybdates at all but at very low fields ($E < 0.01$ kV). It was also observed that both σ and S do not depend upon the dimensions of the pellet. Further, S does not depend upon P and therefore needs no correction.

In order to understand the electrical transport mechanism in the molybdates studied, the electrical conductivity at 1 kHz and the Seebeck coefficient of several pellets of each molybdate were measured with platinum/silver foil electrodes in heating and cooling cycles. It was found that σ values are almost the same in both heating and cooling cycles, but at lower temperatures the cooling-cycle values were found to be smaller than the heating-cycle values. It was also noticed that if a measurement was repeated in more than one successive heating and cooling cycles, the gap between the $\log \sigma$ versus T^{-1} curves narrows. The high σ values in the cooling cycle may reflect boundary oxidation or removal of water molecules present either as moisture or due to hydrate formation. Rare-earth molybdates are hygroscopic [6], and some form hydrates. The higher σ values in the heating cycle thus reflect the presence of water molecules and their slow removal on heating. In view of this cooling-cycle values have been taken as being the more representative values of σ for these molybdates. The graphs of $\log \sigma$ versus T^{-1} for all the molybdates in the cooling cycle are shown in Figs 1–6. It is seen from these figures that the σ values of these molybdates vary from $10^{-8}\,\Omega^{-1}\,m^{-1}$ to $10^{2}\,\Omega^{-1}\,m^{-1}$ in the temperature interval 450–1200 K. Obviously all these molybdates are essentially insulators and become semicon-

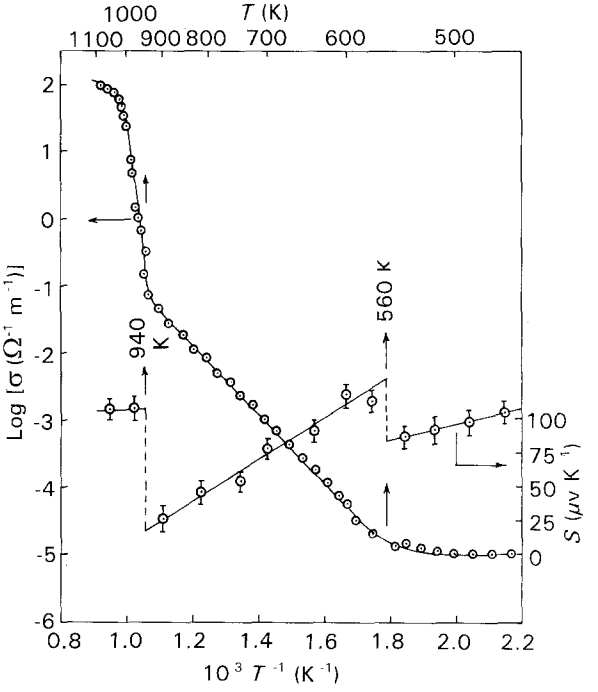

Figure 2 Plots of (⊙) $\log \sigma$ and (⊙) S versus T^{-1} for the cooling cycle of cerium molybdate, $Ce_2(MoO_4)_3$.

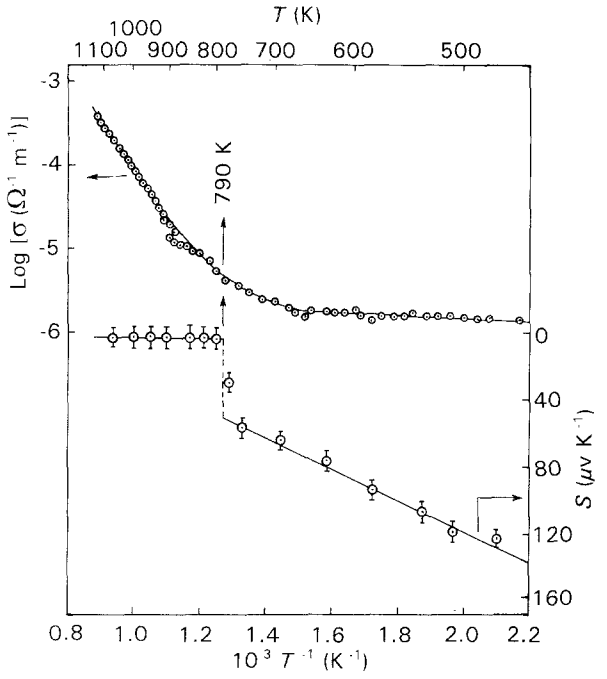

Figure 1 Plots of (⊙) $\log \sigma$ and (⊙) S versus T^{-1} for the cooling cycle of lanthanum molybdate, $La_2(MoO_4)_3$.

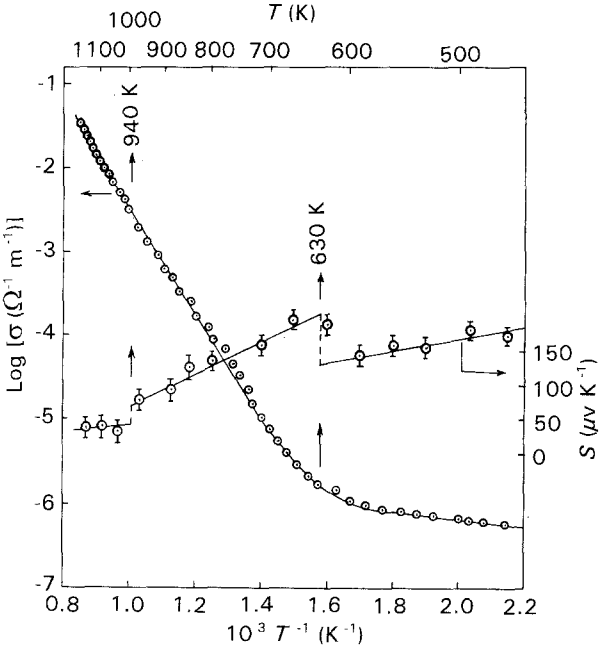

Figure 3 Plots of (⊙) $\log \sigma$ and (⊙) S versus T^{-1} for the cooling cycle of praceodymium molybdate, $Pr_2(MoO_4)_3$.

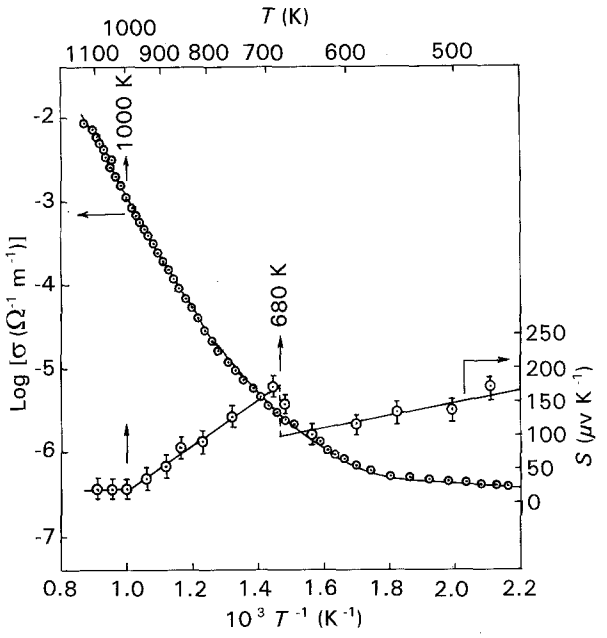

Figure 4 Plots of (⊙) log σ and (⊙) S versus T^{-1} for the cooling cycle of neodymium molybdate, $Nd_2(MoO_4)_3$.

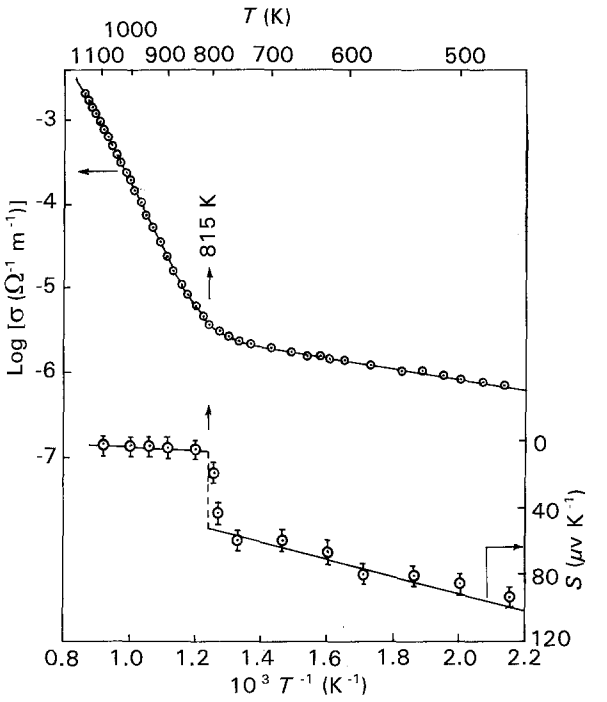

Figure 5 Plots of (⊙) log σ and (⊙) S versus T^{-1} for the cooling cycle of samarium molybdate, $Sm(MoO_4)_3$.

ductors only at higher temperatures. $Ce_2(MoO_4)_3$ seems to attain the highest conductivity of these molybdates ($10^2\ \Omega^{-1}\,m^{-1}$ at 1100 K) but the nature of the conductivity does not appear to be metallic. The log σ versus T^{-1} plots for all the molybdates are quite similar, being straight lines in some regions. These plots can be divided, in general, into three temperature ranges: (i) a linear region for $T < T_1$, (ii) a linear region for $T_1 < T < T_2$, and (iii) a region for $T > T_2$. T_1 and T_2 are temperatures at which either the slope of the plot changes or σ jumps by some factor. These temperatures can be designated as break temperatures. The linear log σ versus T^{-1} plot in each region can be represented by the relation

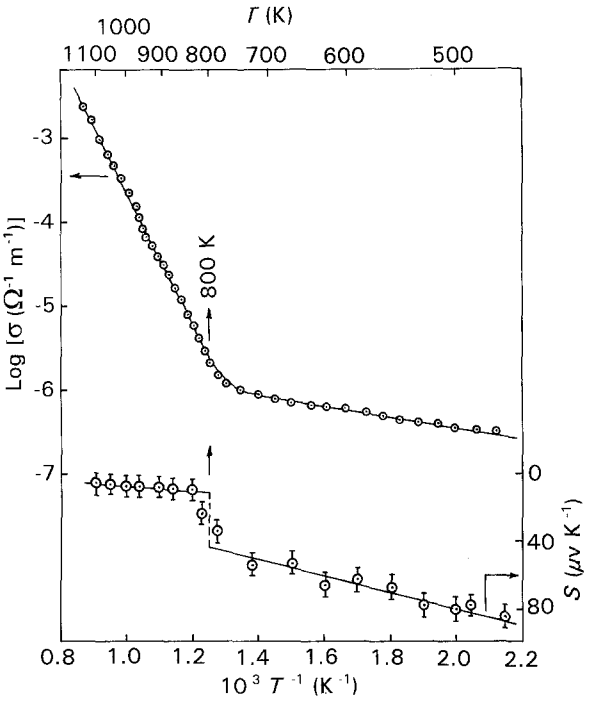

Figure 6 Plots of (⊙) log σ and (⊙) S versus T^{-1} for the cooling cycle of europium molybdate, $Eu_2(MoO_4)_3$.

$$\sigma = \sigma_0(T)\exp(-W/2kT) \quad (1)$$

where σ_0 is a nearly temperature-independent constant and W is the activation energy. Both σ_0 and W have different values for different molybdates. The values evaluated for these constants together with the values of T_1 and T_2 are given in Table I.

The Seebeck coefficient of each molybdate was measured for several pellets in the temperature range 430–1200 K in both heating and cooling cycles. No significant difference was noticed between the cooling- and heating-cycle values. The accuracy of the S measurement depends upon the resistance of the sample pellet. Thus, a typical error in the reported value of S is about $\pm 10\%$. A sign convention can be used in which positive S indicates a negative charge carrier and vice-versa. The results of the S variation with T^{-1} are shown in Figs 1–6 for different molybdates; the curves are quite similar. In general, these curves have three regions. First, $T < T_1'$; secondly, $T_1' < T < T_2'$; and thirdly, $T > T_2'$. In these regions the variation of S with T^{-1} is a straight line which can be represented by the relation

$$S = \eta/eT + H \quad (2)$$

The experimental values of η, H, T_2' and T_1' are given in Table II. A comparison of T_1 with T_1' and T_2 with T_2' reveals small differences between them. These differences are due to the different conditions of measurement used to obtain S and σ. In the former case, the mean value of the temperature does not reflect the true thermal state of the pellet. However, it appears that these temperatures ($T_1 - T_1'$ and $T_2 - T_2'$) reflect the same transition in the sample.

TABLE I Summarized results of electrical conductivity measurement for studied molybdates (general expression $\sigma = C\exp(-W/2kT)$

Material $R_2(MoO_4)_3$ with R =	$T < T_1$			$T_1 < T < T_2$[a]			$T > T_2$	
	C ($\Omega^{-1}m^{-1}$)	W (eV)	T_1 (K)	C ($\Omega^{-1}m^{-1}$)	W (eV)	T_2 (K)	C ($\Omega^{-1}m^{-1}$)	W (eV)
La	3.83×10^{-6}	0.08	790	7.43×10^{1}	2.30	–	–	–
Ce	4.62×10^{-5}	0.12	560	1.33×10^{4}	2.00	940	–	–
Pr	6.72×10^{-6}	0.20	630	5.70×10^{3}	2.50	990	3.38×10^{4}	2.80
Nd	4.70×10^{-6}	0.21	680	1.47×10^{4}	2.80	1000	3.24×10^{4}	2.96
Sm	1.47×10^{-5}	0.24	815	1.05×10^{4}	3.04	–	–	–
Eu	8.89×10^{-6}	0.28	800	2.86×10^{4}	3.20	–	–	–

[a] For La, Sm and Eu, T_2 does not appear.

TABLE II Summarized results of Seebeck coefficient measurement for the studied molybdates $R_2(MoO_4)_3$ [general expression $S = \eta/eT + H$]

R	S at 500 K ($\mu V K^{-1}$)	η (eV)	H ($\mu V K^{-1}$)	T_1' (K)	S at 900 K ($\mu V K^{-1}$)	η (eV)	H ($\mu V K^{-1}$)	T_2' (K)	Charge carrier for both regions (h, hole; e, electron)
La	−120	−0.05	−20.0	790	−3.6	−0.003	+0.3	–	h
Ce	+95	+0.05	−5.0	560	+25.0	+0.150	−140.0	940	e
Pr	+165	+0.08	+5.0	630	+105.0	+0.240	−170.0	990	e
Nd	+145	+0.08	−15.0	680	+80.0	+0.250	−200.00	1000	e
Sm	−90	−0.05	+10.0	815	−5.3	−0.003	−2.0	–	h
Eu	−80	−0.05	+20.0	800	−8.0	−0.002	−5.8	–	h

It can be concluded from the time-dependence study of σ (direct current) that light rare-earth molybdates are essentially electronic semiconductors. Electron (or hole) conduction can be of two types, band type, or hopping type. But the value of the Seebeck coefficient is low and temperature dependent, hence electrical conduction in these molybdates is essentially band type. The energy bands responsible for the electrical conduction in the molybdates are a filled O^{2-}:2p band separated in energy from the Mo^{6+}:4d and R^{3+}:5d bands by a large (e.g. 3 eV) energy gap. Partially filled, extremely narrow R^{3+}:$4f^n$ levels generally have successive $4f^n$ and $4f^{n+1}$ levels separated by an electron correlation splitting, U, that is greater than this gap. Therefore, both the energy levels cannot fall within the band gap simultaneously. However, a filled $4f^n$ or empty $4f^{n+1}$ level may fall within the gap. Magnetic-susceptibility data [30, 34] for these compounds, which are compatible with an R^{3+}:$4f^n$ state, confirms the localization of 4f electrons on the R^{3+} ions. Both the empty Mo^{6+}:4d and R^{3+}:5d bands lie above the O^{2-}:2p filled band and experiment indicates that Mo^{6+} ions are more easily reduced than the R^{3+} ions which would place the Mo^{6+}:4d band lower but with considerable admixture from the R^{3+}:5d states. It follows from this argument that the intrinsic band conduction in rare-earth molybdates can be described by the energy-band model schematically shown in Fig. 7 irrespective of their structural forms.

It can be seen from Table I that the activation energy corresponding to the slope of the $\log\sigma$ versus T^{-1} plot is small ($\sim$0.1 eV) for all the molybdates studied in the temperature range $T < T_1$. Thus this region belongs to extrinsic conduction. However, for $T_1 < T < T_2$, the conduction is expected to be intrinsic. The variations of $\log\sigma$ with T^{-1} in the intrinsic range are quite similar for all the molybdates studied. However, the variations of S with T^{-1} as well as the values of S are not quite similar in all the molybdates

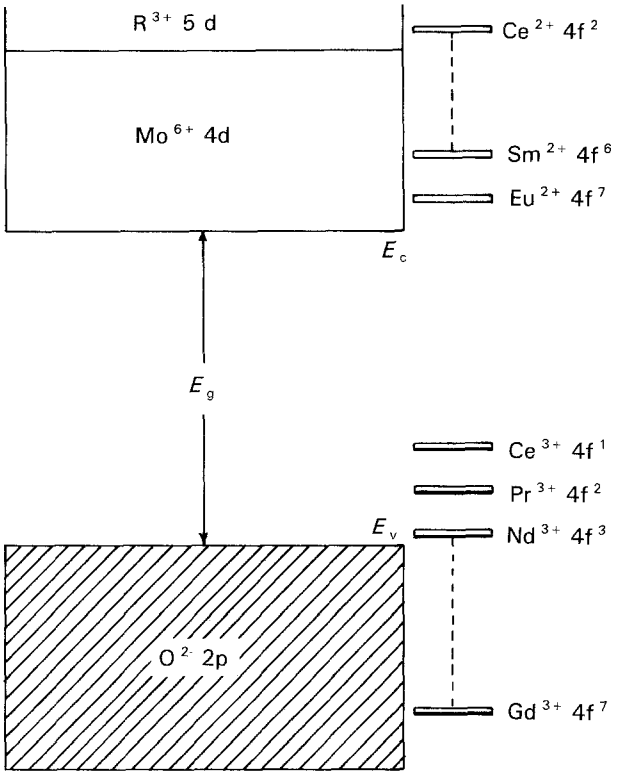

Figure 7 Schematic energy-band diagram for the light rare-earth molybdates studied.

in this temperature range. For La, Sm and Eu molybdates, the values of S are small, positive and nearly independent of temperature (~ 0.002 eV). This rules out the possibility of $4f^n$ or $4f^{n+1}$ levels lying within the energy-band gap [43]. Thus intrinsic conduction in these materials will be due to the thermally generated electrons in Mo^{6+}:4d and holes in O^{2-}:2p bands. Both Mo^{6+}:4d and O^{2-}:2p bands are expected to be wide bands. The expressions for σ and S for electrical conduction in these bands can be given by the following equation [39].

$$\sigma = \sigma_0(T)\exp(-E_g/2kT) \tag{3}$$

with

$$\sigma_0 = 2e\left(\frac{2\pi m_h^* kT}{h^2}\right)^{3/2} a^{3/4}\mu_h(1 + c) \tag{4}$$

where

$$a = m_e^*/m_h^*, \qquad c = \mu_e/\mu_h \tag{5}$$

and the variation of S with temperature is given by the following relation [39]

$$S = \frac{E_g}{2e}\left(\frac{c-1}{c+1}\right)\frac{1}{T} + \frac{2k}{e}\left(\frac{c-1}{c+1}\right) + \frac{3k}{4e}\log_e a \tag{6}$$

where the symbols have their usual meanings. In a broad energy-band model, the variation of μ_e and μ_h and m_e^* and m_h^* with temperature is expected to be small and similar. Hence the ratios a and c are approximately temperature independent. In such a situation, the graph of S versus T^{-1} will be a straight line with a gradient $(E_g/2e)(c - 1/c + 1)$. From the linear $\log\sigma$ versus T^{-1} plots, E_g can be evaluated, and then c can be obtained from the gradient of S versus T^{-1}. Knowing c and the intercept of S on the T^{-1} graph, a can be evaluated. From the known values of c, a and σ_0, μ_e and μ_h can be calculated in terms of m_e^* and m_h^*. The exact values of m_e^* and m_h^* are not known for any of these solids. However, one can estimate the order of μ_e and μ_h by taking the mass of the majority charge carrier to be equal to the mass of a free electron. Computed values of μ_e and μ_h are given in Table III.

For Ce, Pr and Nd molybdates, the values of S are positive for $T_1' < T < T_2'$ indicating that electrons are the majority charge carriers. Further, the values of S as well as the gradient of the S versus T^{-1} graphs is large. This indicates [43] that the $4f^n$ levels in these molybdates lie above the top of the valence O^{2-}:2p band as indicated in Fig. 7. Intrinsic conduction in these solids will occur when electrons from $4f^n$ levels are excited to the Mo^{6+}:4d band, giving electron-dominated conduction. The hole mobility, μ_h, in the $4f^n$ levels will be extremely small and they will be almost localized. In such a case, the effective hole mass $m_h^* \gg m_e^*$. Intrinsic conduction in these solids can be given by the expression

$$\sigma = B(T)\exp(-W/2kT) \tag{7}$$

with

$$B(T) = 2[(2\pi m_e^* kT/h^2)^{3/2}N]^{1/2}\mu_e e \tag{8}$$

where N is the number of lanthanide ions per unit volume, and excitation from the O^{2-}:2p band is neglected. Thus the experimentally obtained straight line plots of $\log\sigma$ versus T^{-1} for these solids can also be justified. In the above equation m_e^* and μ_e are not known. From the known experimental values of $B(T)$, a rough estimate of μ_e can be made taking $m_e^* \simeq m$. These estimated values of μ_e are also given in Table III for Ce, Pr and Nd molybdates. W in these cases will be the difference between the energy at the bottom of the conduction band and the $4f^n$ level.

It can be seen from Table III that mobility of the majority charge carriers in the molybdates studied varies from 10^{-6} to $10^{-4}\,m^2\,V^{-1}\,s^{-1}$. In band conduction the mobility of majority charge carriers is expected to be of the order of $0.1\,m^2\,V^{-1}\,s^{-1}$ or more [44]. Thus the calculated values for mobility are an order of magnitude less than that expected from the normal energy band model. Several reasons lead to a lowering of the mobility of charge carriers such as: grain-boundary effects, narrowing of energy bands by potential fluctuation at high temperature, neglect of electronic correlation in simple energy-band theory, scattering of charge carriers by localized rare-earth magnetic impurities and polaron formation. However, the last of these seems to be the most important in these solids. The theory of polaron formation is very well developed by now [40–42, 44]. As is evident from

TABLE III Charge carrier and evaluated values of mobility for the intrinsic region for molybdates $R_2(MoO_4)_3$

R	W (eV)	C ($\Omega^{-1}\,m^{-1}$)	Charge carrier	W	Mobility ($m^2\,V^{-1}\,s^{-1}$) at 800 K	
					μ_e	μ_h
La	2.30	7.43×10^1	h	$E_c - E_v$	–	2.15×10^{-6}
Ce	2.00	1.33×10^4	e	$E_c - E(4f^1)$	1.12×10^{-4}	–
Pr	2.50	5.70×10^3	e	$E_c - E(4f^2)$		
	2.80	3.38×10^4	e	$E_c - E_v$	2.72×10^{-5}	–
Nd	2.80	1.47×10^4	e	$E_c - E(4f^3)$		
	2.96	3.24×10^4	e	$E_c - E_v$	1.20×10^{-4}	–
Sm	3.04	1.05×10^4	h	$E_c - E_v$	–	1.36×10^{-4}
Eu	3.20	2.86×10^4	h	$E_c - E_v$	–	1.91×10^{-4}

For $W = E_c - E_v$, $C = \sigma_0$ and for $W = E_c - E(4f)$, $C = B(T)$

the magnetic susceptibility data, rare-earth molybdates are ionic solids and therefore the formation of large polarons with intermediate coupling seems to be more reasonable.

Large polarons with intermediate coupling conduct via a band mechanism, but they are largely scattered by longitudinal optical phonons. Their mobility is given by the following expression [42]

$$\mu = \mu_0 \exp(\hbar\omega_0/kT) \quad (9)$$

where ω_0 is the longitudinal optical phonon frequency. The Seebeck coefficient due to large polarons with intermediate coupling also decreases with temperature [44]. Thus the high temperature experimental data for σ and S in all the molybdates studied can be explained quantitatively using the concept of large polarons with intermediate coupling. The effective mass in this case will be much larger than a rigid-band effective mass of the electron and the resulting mobility will be much less than that of a free electron or hole. Using the temperature variation of mobility, W will denote $(E_c - E_v) - 2\hbar\omega_0$ i.e. $W = (E_g - 2\hbar\omega_0)$ for La, Sm and Eu molybdates. For Ce, Pr and Nd molybdates, W will denote $E_c - E(4f^n) - 2\hbar\omega_0$. For rare-earth molybdates, ω_0 is expected to be of the order of 10^{14} Hz [45], which gives $2\hbar\omega_0 \sim 0.13$ eV. Thus the band gap ($E_g = E_c - E_v$) listed in Table III should be larger than this value. Thus E_g for La molybdate becomes 2.43 eV, 3.09 eV for Sm and 3.33 eV for Eu. An energy band gap of $\sim$3 eV has been obtained in heavy rare-earth molybdates [35].

Below T_1 the graph of $\log\sigma$ versus T^{-1} is a good straight line for all the molybdates. The activation energy is very small ($\sim$0.1 eV) and the pre-exponential factor is also low (Table I). This suggests that intrinsic band conduction is not the predominant conduction mechanism in this temperature range. Probably the electrical conduction becomes extrinsic, with impurities playing the significant role. The gradient of the S versus T^{-1} graph shows that the charge carriers are thermally generated. This leads to the probable formation of slightly deep donors or acceptors in these solids.

For Pr and Nd molybdates, a change of gradient of $\log\sigma$ versus T^{-1} occurs at T_2. The gradient above this temperature becomes larger than the gradient below T_2. The reason for this change is that electrical conduction below T_2 is dominated by electrons thermally excited to conduction bands from $4f^n$ levels. Above T_2, the electrons excited from the O^{2-}:2p valence band to the Mo^{6+}:4d conduction band, and the holes thereby generated in the valence band, start dominating the electrical conduction. The slope of the $\log\sigma$ versus T^{-1} graph in such a case will automatically increase. Further, a slight decrease in the values and temperature dependence of S is also expected in such a case, which is quite evident from Figs 3 and 4. If this is true, the slope of $\log\sigma$ versus T^{-1} plot above T_2 will be the energy-band gap of these solids. Thus E_g for Pr and Nd molybdates will be 2.80 eV and 2.96 eV, respectively. If the formation of large polarons with intermediate coupling in these bands and the exponential (Equation 9) temperature variation of mobility are taken into consideration, then the value of the energy-band gap has to be increased by about 0.13 eV. Thus the correct energy-band gap for Pr and Nd molybdates will be 2.93 eV and 3.09 eV, respectively. There is no change in the gradient of $\log\sigma$ versus T^{-1} for La, Sm and Eu molybdates from T_1 to 1200 K. Thus T_2 does not exist for these solids. This is quite understandable in view of the fact that no structural phase transition is reported for these materials below 1200 K, and the energy-band picture does not predict any change in the conduction mechanism. In the light of above discussion, $Ce_2(MoO_4)_3$ is expected to have a similar type of conduction mechanism to that predicted for Pr and Nd molybdates. In such a situation, a change and increase in the gradient of $\log\sigma$ versus T^{-1} around T_2 is expected. However, in this material the σ value increases very rapidly around T_2. In fact, within a span of 50 K, σ jumps by a factor of 150 and becomes of the order of 80 $\Omega^{-1}\,m^{-1}$. The conductivity thus falls within the semimetal range. Thus a semiconductor–semimetal transition is witnessed in this material around 940 K. The reason for this unique behaviour of cerium molybdate is the multivalent character of cerium. This material exists in trivalent as well as tetravalent states; thus at higher temperatures it may change from a Ce^{3+} state to a Ce^{4+} state giving a large number of electrons and a metallic state to the material.

Acknowledgement

The authors thank CSIR of India for financial assistance.

References

1. H. J. BORCHARDT and P. E. BIERSTEDT, *J. Appl. Phys.* **38** (1967) 2057.
2. L. E. CROSS, A. FOUSKOVA and S. E. CUMMINS, *Phys. Rev. Lett.* **21** (1968) 812.
3. P. B. JAMIESON, S. C. ABRAHAMS and J. L. BERNSTEIN, *J. Chem. Phys.* **50** (1969) 86.
4. K. AIZU, A. KUMADA, H. YOMOTO and S. ASHIDA, *J. Phys. Soc. Jpn.* **27** (1969) 511.
5. R. E. NEWNHAM, H. A. MCKINSTRY, C. W. CREGG and W. R. STITT, *Phys. Status Solidi* **32** (1969) 49.
6. K. NASSAU, J. W. SHIRVER and E. T. KEVE, *J. Solid State Chem.* **3** (1971) 411.
7. R. C. MILLER, W. A. NORDLAND and K. NASSAU, *Ferroelectrics* **2** (1971) 97.
8. L. H. BRIXNER, P. E. BIERSTEDT, A. W. SLEIGHT and M. S. LICIS, *Mater. Res. Bull.* **6** (1971) 545.
9. L. H. BRIXNER, A. W. SLEIGHT and M. S. LICIS, *J. Solid State Chem.* **5** (1972) 247.
10. L. H. BRIXNER, J. R. BARKLEY and W. JEITSCHKO, 'The hand book on the physics and chemistry of rare-earths' Vol. 3, Non-metallic Compounds, edited by K. A. Gschneidner Jr and L. Eyring (North Holland, Amsterdam, 1979), p. 610.
11. H. B. LAL, B. K. VERMA and N. DAR, *India J. Cryogenics* **2** (1977) 199.
12. H. B. LAL, V. PRATAP and A. KUMAR, *Pramana* **4** (1978) 409.
13. B. K. VERMA, V. PRATAP and H. B. LAL, *Indian J. Pure Appl. Phys.* **18** (1980) 150.
14. H. B. LAL, N. DAR and A. KUMAR, *J. Phys. C* **7** (1974) 4335.
15. *Idem., ibid.* **8** (1975) 2745.
16. H. B. LAL and N. DAR, *Physica B* **84** (1976) 254.
17. H. B. LAL and N. DAR, *Mater. Res. Bull.* **14** (1979) 1263.

18. H. B. LAL, *J. Mag. Mag. Mater.* **23** (1981) 41.
19. H. B. LAL and M. SINGH, *J. Phys. C* **15** (1982) 291.
20. H. B. LAL, B. K. VERMA and V. R. YADAV, *J. Mater. Sci.* **17** (1982) 3317.
21. V. R. YADAVA, B. K. VERMA, A. K. TRIPATHI and H. B. LAL. *Z. Naturforsch* **37a** (1982) 1083.
22. H. B. LAL and S. METHFESSEL, *J. Mag. Mag. Mater.* **23** (1981) 283.
23. H. B. LAL, *J. Mag. Mag. Mater.* **30** (1982) 192.
24. A. K. TRIPATHI and H. B. LAL, *Mater. Res. Bull.* **12** (1980) 233.
25. A. K. TRIPATHI and H. B. LAL, *J. Mater. Sci.* **17** (1982) 1595.
26. K. GAUR, A. K. TRIPATHI and H. B. LAL, *J. Mater. Sci. Lett.* **2** (1983) 161.
27. *Idem., ibid.* **2** (1983) 371.
28. K. GAUR and H. B. LAL, *J. Mater. Sci. Lett.* **2** (1983) 744.
29. K. GAUR and H. B. LAL, *J. Mater. Sci.* **19** (1984) 3325.
30. H. B. LAL and R. N. PANDEY, *Z. Naturforsch* **330** (1978) 235.
31. R. N. PANDEY, V. PRATAP and H. B. LAL, *Proc. Nat. Acad. Sci. India A* **48** (1978) 1.
32. V. PRATAP and H. B. LAL, *Nat. Acad. Sci. Lett. India* **1** (1978) 381.
33. A. K. TRIPATHI and H. B. LAL, *J. Phys. Soc. Jpn.* **49** (1980) 1896.
34. H. B. LAL and V. PRATAP, *J. Mater. Sci.* **17** (1982) 377.
35. V. PRATAP, K. GAUR and H. B. LAL, *Mater. Res. Bull.* **22** (1987) 1381.
36. A. K. TRIPATHI, PhD thesis, Gorakhpur University (1981).
37. K. GAUR, PhD thesis, Gorakhpur University (1984).
38. R. KUMAR, *Sci. Reporter* **8** (1971) 568.
39. T. C. HERMAN and J. M. HONIG, "Thermoelectric and thermomagnetic effects and applications" (McGraw-Hill, New York, 1967) p. 142.
40. J. APPEL, *Solid St. Phys.* **21** (1968) 193.
41. J. G. AUSTIN and N. F. MOTT, *Adv. Phys.* **18** (1969) 41.
42. A. J. BOSMAN and H. J. VANDALL, *Adv. Phys.* **19** (1970) 1.
43. H. B. LAL and KANCHAN GAUR, *J. Mater. Sci.* **23** (1988) 919.
44. H. J. SUMI, *Phys. Soc. Jpn.* **33** (1972) 327.
45. E. V. DUPLEPOV, S. S. BOTSANOV and G. N. KVSTOVA, *J. Struct. Chem. U.S.A.* **13** (1972) 871.

Received 18 February
and accepted 10 December 1992